Paper ID APEN-MIT-2021_61
Applied Energy Symposium: MIT A+B
August 11-13, 2021 • Cambridge, USA

Optimized Autonomous Driving: an Energy Component Analysis

Eduardo Mello
Department of Electrical Engineering
University of Notre Dame
Notre Dame, USA
emello@nd.edu

Matthew Peine
Department of Electrical Engineering
University of Notre Dame
Notre Dame, USA
mpeine@nd.edu

Peter Bauer
Department of Electrical Engineering
University of Notre Dame
Notre Dame, USA
pbauer@nd.edu

Abstract—An energy components analysis for stop-to-stop drive segments is provided. In particular, the components of rolling resistance, air drag, and kinetic energy are examined for conventional and optimal segments. It is shown that in energy-optimal driving, the maximum kinetic energy is reached early in the drive segment and then it is converted into work to overcome air drag and rolling resistance; in a sense, it is recovering kinetic energy. In conventional profiles, the maximum speed is attained late in the profile and thus cannot be used to cover much of the air drag and rolling resistance energy cost. The role of the initial acceleration is shown to play a key role, especially for short segments. These results are illustrated through several simulation examples.

Keywords—optimization, energy, autonomous driving, acceleration

I. INTRODUCTION

Recent advances in autonomous driving, electric powertrains, and situational awareness acquisition provide unprecedented opportunities for maximizing sustainability in transportation. The high efficiency of electric powertrains (from battery to wheel), the ability to execute and generate optimal speed trajectories due to autonomous driving systems, and the ability to acquire real-time traffic and infrastructural data (via V2X or internal sensor suites) set the stage for many advances in the area of transportation, opening a new era of transportation. Many results that use infrastructural and vehicle information to optimize energy already exist; only some of the many recent results obtained can be mentioned here. Most notably, energy optimal speed control systems for signalized arterials have been proposed by several authors. These systems aim to achieve energy savings by minimizing the number of stops at traffic lights, reducing idling times [1,2]. These strategies are often called "green driving" or "eco-driving." These algorithms can also consider the length of intersection queues [3], or vehicle dynamics throughout the entire time horizon [4].

This paper will further pursue the approach in [5,6], which showed that significant efficiency gains are possible if stop-to-stop trajectories are optimized using constraints on average speed, maximum acceleration and deceleration, and possibly additional constraints. While [5,6] focused on the efficiency gains as a function of infrastructural and vehicle parameters, the research did not explain why such high energy savings (sometimes around 50-60%) are possible. It also did not investigate the role that acceleration plays in such energy improvements. These two issues are closely related, and this paper will shed some light on the interdependency of initial acceleration, total energy savings or efficiency gains, and the energy components that contribute to these savings.

This paper will provide fundamental insights into how the three different energy components caused by air drag, rolling resistance, and kinetic energy depend on the initial acceleration. A theoretical analysis as well as a simulation study will highlight the relationship between initial acceleration and these energy components. It will be shown that a high initial acceleration capability is advantageous for improving energy efficiency, which seems counterintuitive when considering conventional ICE vehicles.

In section 2, the utilized energy, efficiency, and optimization models will be introduced. Section 3 provides an energy component analysis from an analytical as well as a simulation point of view. In section 4, the dependency of transportation energy on initial acceleration is shown. Finally, section 5 provides conclusions and an outlook.

II. MODELS

A. Energy models and assumptions

The energy consumption of an electric vehicle is estimated based on the wheel power P_{wheel}, which can be described as the sum of all power absorbing components acting on the vehicle (1) [5,7]. Those components comprise the acceleration power P_{acc} (2), power necessary to overcome air-drag P_{air} (3), power necessary to overcome rolling resistance P_{roll} (4), and power necessary for hill-climbing P_{hill} (5). For the analysis presented below, a flat surface was considered, i.e., no hill-climbing, and zero wind speed, i.e., $w(t) = 0$.

$$P_{wheel}(t) = P_{acc} + P_{air} + P_{roll} + P_{hill} \quad (1)$$

$$P_{acc} = mv(t)\dot{v}(t) \quad (2)$$

$$P_{air} = \frac{1}{2} C_d A \rho \big(v(t) + w(t)\big)^2 v(t) \quad (3)$$

$$P_{roll} = mgf_r v(t) \quad (4)$$

$$P_{hill} = mgsin(\alpha)v(t) \quad (5)$$

Above, the mass, speed, acceleration, frontal drag coefficient, and cross-sectional area of the vehicle are denoted by m, v, $\dot{v}$, C_d, and A, respectively. The vehicle mass also models the driveline inertia, which appears as a constant additional mass contribution, i.e., a single gear transmission is

assumed [8]. $w(t)$ is the component of wind speed aligned with the vehicle's velocity vector. The air density is denoted by ρ, f_r is the rolling resistance coefficient, and g is the gravitational acceleration.

The battery power drawn is then obtained by multiplying the power at the wheels by the total drivetrain efficiency (6).

$$P_{bat}(t) = \begin{cases} \eta_{frw}(T,\omega)^{-1} P_{wheel}(t) \text{ for } P_{wheel}(t) \geq 0 \\ \eta_{reg}(T,\omega) P_{wheel}(t) \text{ for } P_{wheel}(t) < 0 \end{cases} \quad (6)$$

where P_{bat} is the power at the battery, η_{frw} is the efficiency of the vehicle for forward power flow, η_{reg} is the efficiency in reverse power flow, T is the torque of the motor, and ω is the rotational speed of the motor. These efficiencies represent the complete powertrain efficiency, including the mechanical drivetrain and battery efficiency, which, as shown in [8], have minimal variations under different operating conditions.

In the following sections, the vehicle efficiency will be obtained from the torque- and speed-dependent efficiency map shown in Fig. 1. Each vehicle will utilize a scaled version of this map that matches the vehicle's maximum torque and motor speed. This efficiency map is derived from a Nissan Leaf's combined motor and inverter efficiency [9].

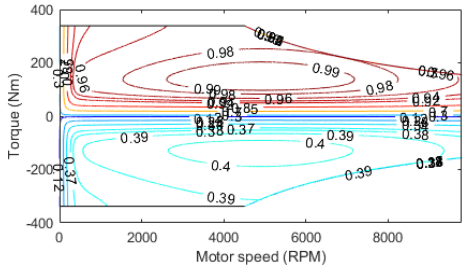

Fig. 1. Example of efficiency map utilized in the optimization.

Finally, the total energy drained from the battery, E, is given by (7) where t_i and t_f are the initial and final time of drive segment, respectively.

$$E = \int_{t_i}^{t_f} P_{bat}(t)dt \quad (7)$$

B. Optimization models and assumptions

To find the optimal speed profile between two consecutive stops, e.g., a segment between traffic lights or stop signs, of an urban scenario, an optimization problem with energy as the only parameter in the cost function will be solved. This optimization problem is formulated below (8).

$$\begin{aligned} &\underset{v(t)}{minimize} \int_0^{t_f} P_{bat}(\tau)d\tau \\ &s.t. \frac{\int_0^{t_f} v(\tau)d\tau}{t_f} = \bar{v} \\ &0 \leq v(t) \leq v_{max} \\ &\dot{v}_{min} \leq \dot{v}(t) \leq \dot{v}_{max} \end{aligned} \quad (8)$$

In this optimization, the average speed of the vehicle $\bar{v}$, speed limitations, and acceleration limits are defined as constraints. In (8), t_f is the total optimization time, v_{max} is the maximum acceptable speed, and $\dot{v}_{min}$ and $\dot{v}_{max}$ are the minimum and maximum acceptable acceleration values. More constraints may have to be imposed, depending on the application, e.g., speed boundary conditions.

III. Energy Component Analysis

The generation of energy-optimal speed profiles and their energy consumption has been studied in [5,6]. However, the reason for these large savings has not been analyzed. Here, this analysis will be performed by breaking down the energy consumption into its power absorbing components.

These energy-optimal speed trajectories can be divided into two different types: three-segment trajectories and four-segment trajectories. Typically, optimal speed trajectories have three distinct segments for short optimized trajectories and four segments for longer speed trajectories [5]. Below a closed-form approximation of a three-segment optimal speed profile will be presented. It is also shown how its energy breakdown behaves as vehicle parameters are varied.

A. Analytical results and the simplified model

For the case of three-segment optimal speed profiles, the closed-form expressions below will be shown to provide a good linear approximation of the optimal speed profile (shown in Fig. 2).

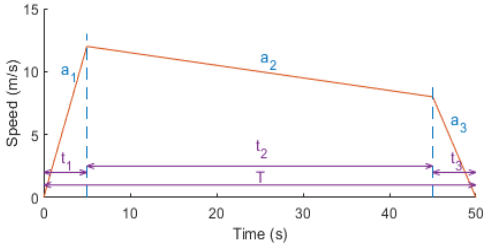

Fig. 2. Sample trajectory for closed-form approximation of a three-segment optimal speed profile.

For this analysis, the parameter $\bar{v}$ represents the average speed of the optimal trajectory, d the segment length, a$a_1 = \dot{v}_{max}$ the initial acceleration, a_2 the approximated coasting deceleration, and $a_3 = \dot{v}_{min}$ the braking deceleration. The indices show the segment number with which the acceleration or time is affiliated, e.g., a_1 and t_1 are acceleration and duration of segment 1.

Based on the integral of the speed profile depicted by Fig. 2, the total traveled distance is given by (9).

$$d = \underbrace{\frac{a_1}{2}t_1^2}_{\substack{\text{distance} \\ \text{covered} \\ \text{in } t_1}} + \underbrace{\frac{2a_1t_1+a_2t_2}{2}t_2}_{\substack{\text{distance} \\ \text{covered} \\ \text{in } t_2}} + \underbrace{\frac{a_1t_1+a_2t_2}{2}t_3}_{\substack{\text{distance} \\ \text{covered} \\ \text{in } t_3}} \quad (9)$$

The total time of the trajectory is defined by (10), where T represents the total travel time. Since the speed trajectory starts and stops at zero speed, (11) must also hold.

$$t_1 + t_2 + t_3 = T = \frac{d}{\bar{v}} \quad (10)$$

$$a_1t_1 + a_2t_2 + a_3t_3 = 0 \quad (11)$$

With some algebraic manipulation, the expressions (12) to (14) for the times t_1, t_2, and t_3 can be obtained. Also, based on the average force acting at the wheels of the vehicle, a_2 can be defined as shown in (15).

$$t_1 = \frac{t_2(a_3-a_2)-a_3T}{a_1-a_3} \quad (12)$$

$$t_2 = \sqrt{\frac{2d(a_1-a_3)+a_1a_3T^2}{(a_1-a_2)(a_3-a_2)}} \quad (13)$$

$$t_3 = T - t_1 - t_2 \quad (14)$$

$$a_2 = -gf_r - \frac{1}{2}\frac{C_dA}{m}\rho\bar{v}^2 \quad (15)$$

Finally, assuming that the vehicle only utilizes energy during t_1, the total energy consumption of the trajectory can be estimated by (16). This assumption is based on the vehicle coasting during t_2 and regenerative braking during t_3.

$$E_{bat} = \frac{ma_1t_1^2}{2\eta}(a_1 + gf_r) + \frac{C_dA\rho a_1^3t_1^4}{8\eta} \quad (16)$$

In the equations above, η is the power train lumped forward efficiency. (Regenerative braking efficiency is assumed to be zero.) The variables g, f_r, C_d, A, ρ, and m represent the following vehicle and environmental parameters: gravitational acceleration, rolling resistance coefficient, air-drag coefficient, vehicle's frontal area, air density, and vehicle's mass, respectively. Finally, the energy utilized by the vehicle is denoted by E_{bat}.

B. Simulations of optimized and conventional trajectories

The closed-form approximation approach above was applied to segments varying in range from 300 to 800 meters. Their estimated energy consumption for a vehicle based on the chassis data of a Nissan Leaf is shown in Fig. 3. In this figure, the set "Closed-form approximation (estimated energy)" represents the results obtained by (16). The set "Closed-form approximation (calculated energy)" represents the energy consumption calculated based on a linearized version of the model described in section II. A. By comparing these two sets, one can assert that (16) produces very close approximations of the energy consumption of an optimal trajectory, especially for short segments. Also, the approximated optimal speed trajectories have very similar energy consumption to those obtained from the optimization scheme described in section II. B, although a little higher. The set "Distilled FTP75" represents a speed profile generated from the FTP75 with the desired segment length. This set is explained in detail in [5].

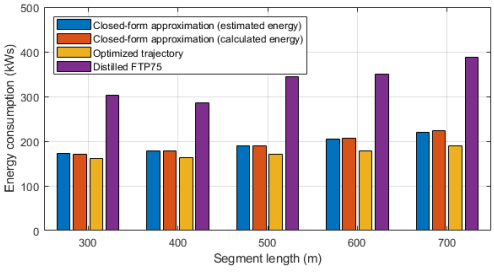

Fig. 3. Energy savings obtained with the closed-form approximation of optimal speed profiles compared to the results from the optimization.

C. Breakdown of components

To analyze the origin of the savings obtained from the energy-optimal speed trajectories, the work realized by the vehicle, i.e., energy at the wheels, was broken down into each one of its power absorbing components. The work realized by the vehicle does not consider the vehicle's efficiency, and thus each component can be expressed as shown below. The total energy necessary to accelerate the vehicle (17), to overcome air drag (18), and to overcome rolling resistance (19) is described. Since a flat surface is assumed, $E_{hill} = 0$.

$$E_{kinetic} = \int_0^{t_f} \max(0, mv(t)\dot{v}(t))\,dt \quad (17)$$

$$E_{air} = \int_0^{t_f} \frac{1}{2}C_dA\rho v^3(t)\,dt \quad (18)$$

$$E_{roll} = \int_0^{t_f} mgf_rv(t)\,dt \quad (19)$$

Equation (20) expresses the total energy that can possibly be recaptured, E_{recap}. This includes energy dissipated by the brakes and the energy sent back to the battery.

$$E_{recap} = \int_0^{t_f} |\min(0, P_{wheel}(t))|\,dt \quad (20)$$

The total energy, at the wheels, recovered to overcome air drag and rolling resistance is then given by (22)

$$E_{recovered} = E_{kinetic} - E_{recap} \quad (21)$$

Fig. 4 shows the speed trajectory, the cumulative energy consumption (at the battery), and the breakdown of the work for the segment length of 300 meters shown in Fig. 3. In this analysis, the energy consumption, Fig. 4(b), was calculated by assuming 80% of forward power flow and no regenerative braking. This graph also shows how the energy consumption of the optimal trajectory and the closed-form approximation are very similar to each other. The main difference between the two is that the optimal trajectory utilizes coasting while the linear approximation may be either accelerating or braking slightly for the second segment of the trajectory.

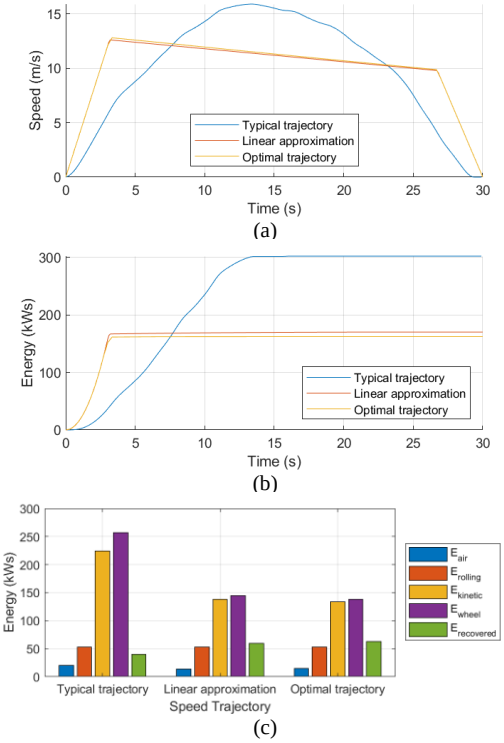

Fig. 4. (a) Speed trajectories, (b) cumulative energy consumption, and (c) breakdown of energy components in a 300-meter segment.

By comparing the "Linear approximation" to the "Typical trajectory" (distilled from the FTP75) in Fig. 4, one can conclude that most of the savings originate from the "Linear approximation" and the "Optimal trajectory" reaching much lower maximum speeds, significantly reducing the energy component necessary to accelerate the vehicle, $E_{kinetic}$ in Fig. 4(c). While the "Typical trajectory" utilizes energy for half of the total time, the "Optimal trajectory" and its linearization

only utilize a significant amount of energy for the first 3.5 seconds. This is possible due to the high investment in kinetic energy at the beginning of the trajectory by the optimizer. In the second and third segments, the accumulated kinetic energy is utilized to overcome air drag and rolling resistance. Looking at Fig. 4(c), the last set of bars (in green) represents the kinetic energy recovered to overcome the air drag and rolling resistance as expressed in (21). This process works as a type of regenerative braking. However, since this recovery acts directly on the energy at the wheels, it operates at 100% efficiency, much higher than actual regenerative braking.

Fig. 5 shows the energy breakdown for two more segment lengths, 500 and 700-meters. The same trends are seen for every segment length, with the linear approximation and optimized trajectories utilizing much more of their kinetic energy to overcome air drag and rolling resistance.

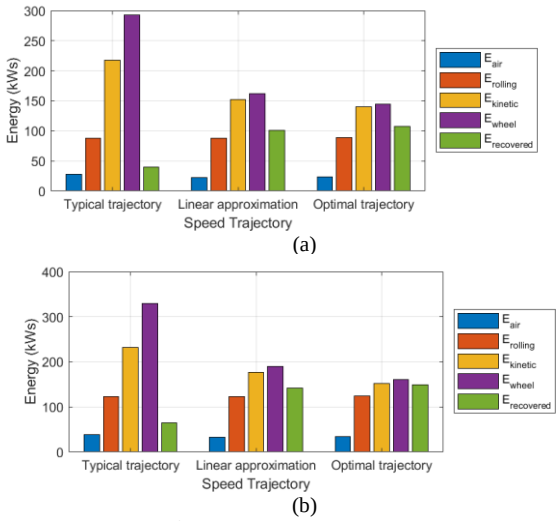

(a)

(b)

Fig. 5. Breakdown of energy components in a (a) 500-meter segment and a (b) 700-meter segment.

D. Regenerative braking vs. energy recovery

By utilizing the energy invested in accelerating the vehicle to overcome air-drag and rolling resistance, the optimal speed profile and their linear approximations can achieve high energy savings. This can be considered a form of regenerative braking. As this process involves neither the mechanical nor the electrical drivetrain, it is not affected by their efficiencies and thus can be considered lossless.

To analyze how effective this energy recovery is, it will be compared to actual regenerative braking. Fig. 6 shows the energy consumption of each one of the three speed trajectories previously introduced ("Typical trajectory," "Linear approximation," and "Optimal trajectory") for segment lengths of 300 meters, 500 meters, and 700 meters. These

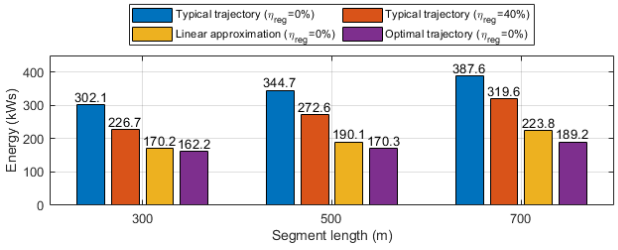

Fig. 6. Energy consumption of each of the trajectories shown in section III-C for a vehicle with 85% of forward motion efficiency and two values of regenerative braking efficiency.

results utilize a vehicle based on the chassis data of a Nissan Leaf with 85% of forward motion efficiency. The set "Typical trajectory ($\eta_{reg} = 40\%$)" utilizes 40% of regenerative braking efficiency while the other sets utilize 0% of regenerative braking efficiency. All the efficiency values are assumed to be constant and represent the overall efficiency from the battery to the wheels and vice versa.

Table I shows the percentage savings obtained by the vehicle compared to the consumption of the "Typical trajectory ($\eta_{reg} = 0\%$)". These results validate the hypothesis that, since the energy recovery obtained from optimal speed trajectories occurs at the wheels, it is more effective than actual regenerative braking. This is demonstrated by the fact that the "Typical trajectory" utilizing 40% of regenerative braking efficiency only managed to recover, on average, 21.15% of the transportation energy of the trajectory extracted from the FTP75. In contrast, the "Linear approximations" and the "Optimal trajectories" averaged 43.60% and 49.36%, respectively (without using traditional regenerative braking). This makes optimization a preferred method for minimizing transportation energy in comparison to traditional regenerative braking. However, in an ideal world, both strategies would be used in combination.

TABLE I. PERCENTAGE SAVINGS COMPARED TO THE TYPICAL TRAJECTORY WITHOUT REGENERATIVE BRAKING

Speed trajectory	**Percentage savings**		
	300-meter	***500-meter***	***700-meter***
Typical trajectory ($\eta_{reg} = 0\%$)	0.00%	0.00%	0.00%
Typical trajectory ($\eta_{reg} = 40\%$)	24.96%	20.94%	17.55%
Linear approximation	43.66%	44.86%	42.27%
Optimal trajectory	46.29%	50.62%	51.18%

IV. THE ROLE OF ACCELERATION IN ENERGY-OPTIMAL TRAJECTORIES

It was previously demonstrated that, in stop-to-stop traffic, high accelerations can provide higher savings in optimal speed profiles [6]. Hence, several simulations based on the three-segment speed profile depicted in Fig. 2 were performed. For this analysis, the initial acceleration was the only parameter changed to determine its role on transportation energy. These calculations were performed for vehicle models based on the chassis data of a Tesla Model S and a Nissan Leaf over distances of 300, 500, and 700 meters.

The mathematical modeling shown in section III. B was utilized with lumped constant efficiency values. The total energy expenditure for the trajectories is given by equation (16). The estimated battery energy for initial accelerations varying from 1m/s^2 to 10m/s^2 are shown in Fig. 7. From this data, two conclusions can be made. First, both

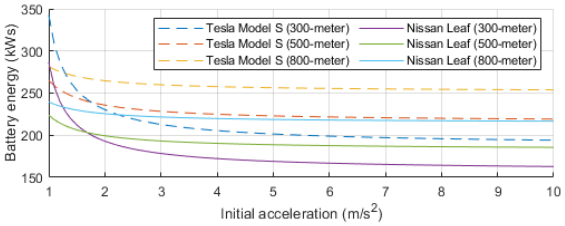

Fig. 7. Estimated energy consumption of both vehicles as a fucntion of the initial acceleration.

vehicles show poor energy consumption for low accelerations in short segments. This is because they spend most of the trajectory in the acceleration phase. Second, both vehicles achieve most of their saving by 4m/s^2 of initial acceleration; diminished returns are observed with higher accelerations.

A. *Comparison to optimization*

To better understand the energy consumption depicted in Fig. 7, the estimated energy obtained above was compared to the consumption obtained by a linearized version of the model in section II. A (here named *calculated energy*). In Fig. 8, for the vehicle based on the chassis data of a Nissan Leaf, the estimated energy consumption is plotted alongside the calculated energy of the same trajectory and the energy consumption of optimized trajectories as described in section II. B (utilizing 85% of forward power flow efficiency and no regenerative braking). Similar data is plotted in Fig. 9 for the vehicle based on the chassis data of a Tesla Model S.

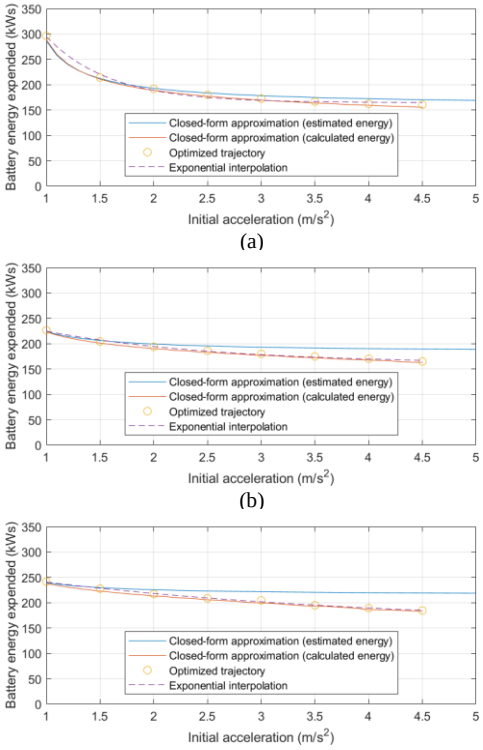

Fig. 8. Energy consumption for a vehicle based on a Nissan Leaf with 85% of constant forward motion efficiency and no regenerative braking for segment lengths of (a) 300, (b) 500, and (c) 700 meters.

From these plots, one can conclude that the estimated energy consumption, the calculated energy consumption of the closed-form approximation, and the optimized trajectories' consumption are very close for short segments. Also, the estimated energy consumption's accuracy deteriorates as the segment length increases, especially for high accelerations. However, in all scenarios, the calculated energy of the linear approximation shows remarkably close energy consumption to the optimal trajectory's consumption.

The previous section observed diminishing returns for accelerations greater than 4m/s^2 for all segment lengths. In contrast, the optimized trajectories still observe significant savings for high accelerations in longer segments, especially for the more powerful Tesla Model S-based vehicle. The maximum speed is achieved earlier with higher accelerations, allowing for extended periods where the accumulated kinetic

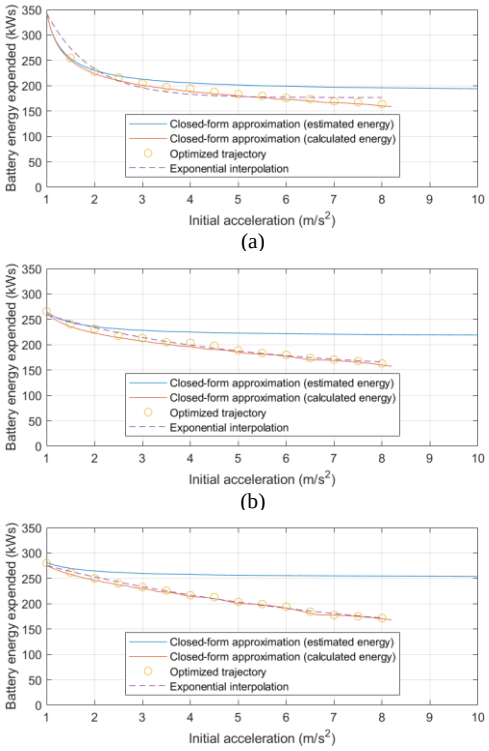

Fig. 9. Energy consumption for a vehicle based on a Tesla Model S with 85% of constant forward motion efficiency and no regenerative braking for segment lengths of (a) 300 meters, (b) 500 meters, and (c) 700 meters.

energy is used to overcome air drag and rolling resistance. High accelerations also lower the maximum speed and thus the kinetic energy for a given average speed constraint.

B. *Utilizing efficiency maps*

A similar analysis is shown with the energy consumption calculated based on a speed- and torque-dependent efficiency map, as shown in Fig. 1 (both forward powerflow and regenerative braking efficiencies are described). The lines in blue still represent the estimated energy consumption, with identical numbers to what is shown in Fig. 8 and Fig. 9.

When utilizing this efficiency model, the diminished returns over 4m/s2 accelerations are present again. However, the energy consumption assumes a more linear behavior for longer segments with the Nissan Leaf-based vehicle (Fig. 10). The vehicle based on the Tesla Model S (Fig. 11) once more shows similar behavior to the Nissan Leaf-based vehicle. While the linear approximation still presents remarkably similar calculated energy consumption to the optimal speed trajectories, the deviation between the two increases in long segments. This is especially true for the Tesla-based vehicle. This happens due to the wide efficiency map of the vehicle, for which the optimizer can take advantage of high-efficiency operating points. Nevertheless, the energy advantage observed by the optimized trajectories comes with the cost of computational complexity. Approximated trajectories have a significantly lower computational complexity than the optimized trajectories.

For both vehicles, the optimization achieves significantly better results than the estimated consumption in all tested accelerations (not only for high acceleration). Thus, making the estimation not a suitable tool to accurately predict the energy consumption of a linear approximation of an energy-optimal speed trajectory when efficiency maps are utilized.

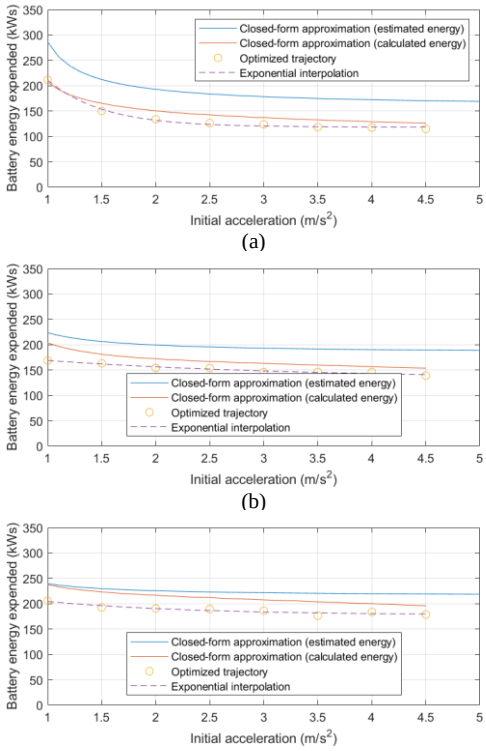

Fig. 10. Energy consumption for a Nissan Leaf utilizing efficiency maps and regenerative braking for segment lengths of (a) 300 meters, (b) 500 meters, and (c) 700 meters.

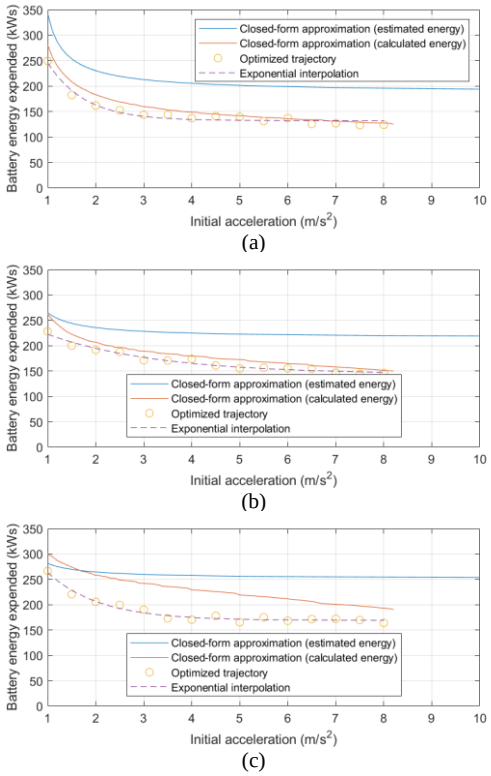

Fig. 11. Energy consumption for a Tesla Models S utilizing efficiency maps and regenerative braking for segment lengths of (a) 300 meters, (b) 500 meters, and (c) 700 meters.

V. Conclusion

The performed energy component analysis for stop-to-stop drive segments revealed several interesting insights. Most importantly, it shows that energy-optimal trajectories achieve significant efficiency gains over conventional speed trajectories (as derived from the FTP75 cycle) by lowering the kinetic energy component and recovering more energy from stored kinetic energy to overcome rolling resistance and air drag later in the trajectory. In a sense, this is similar to regenerative braking. However, here, the regenerated energy is directly recovered to overcome air drag and rolling resistance, i.e., there are no losses from moving energy from the wheel to the battery and vice versa. This and the fact that powertrain efficiency is typically higher under high-performance situations (i.e., hard accelerations) are the main underlying reasons why energy optimization of stop-to-stop segments can reduce total expended energy by over 50%.

One particularly interesting aspect of energy-optimized trajectories is the initial acceleration's role: The higher the acceleration capability, the earlier the maximum speed is achieved and the longer the accumulated kinetic energy can be used to cover energy expenses later in the trajectory. High acceleration also lowers the maximally attained speed and, therefore, the kinetic energy component while keeping the average speed constraint. Hence a high acceleration capability can aid in reducing transportation energy in urban environments. We saw that vehicles achieved most energy savings by around an initial acceleration of $4 m/s^2$.

Even though the energy-optimal trajectories can have a significant energy advantage over the linear approximation (which is more pronounced for powerful drivetrains), the linear approximation's computational complexity still makes them an attractive option for real-world implementation.

References

[1] S. Mandava, K. Boriboonsomsin and M. Barth, "Arterial velocity planning based on traffic signal information under light traffic conditions," *2009 12th International IEEE Conference on Intelligent Transportation Systems*, 2009, pp. 1-6, doi: 10.1109/ITSC.2009.5309519.

[2] G. Mahler and A. Vahidi, "Reducing idling at red lights based on probabilistic prediction of traffic signal timings," *2012 American Control Conference (ACC)*, 2012, pp. 6557-6562, doi: 10.1109/ACC.2012.6314942.

[3] X. Wu, X. He, G. Yu, A. Harmandayan and Y. Wang, "Energy-Optimal Speed Control for Electric Vehicles on Signalized Arterials," in *IEEE Transactions on Intelligent Transportation Systems*, vol. 16, no. 5, pp. 2786-2796, Oct. 2015, doi: 10.1109/TITS.2015.2422778.

[4] X. Qi, G. Wu, P. Hao, K. Boriboonsomsin and M. J. Barth, "Integrated-Connected Eco-Driving System for PHEVs With Co-Optimization of Vehicle Dynamics and Powertrain Operations," in *IEEE Transactions on Intelligent Vehicles*, vol. 2, no. 1, pp. 2-13, March 2017, doi: 10.1109/TIV.2017.2708599.

[5] E. F. Mello and P. H. Bauer, "Energy-Optimal Speed Trajectories Between Stops," in *IEEE Transactions on Intelligent Transportation Systems*, vol. 21, no. 10, pp. 4328-4337, Oct. 2020, doi: 10.1109/TITS.2019.2939776.

[6] E. F. Mello and P. H. Bauer, "Energy-optimal Speed Trajectories between Stops and Their Parameter Dependence," *5th International Conference on Vehicle Technology and Intelligent Transport Systems (VEHITS)*, 2019, pp. 513-520, doi: 10.5220/0007747605130520.

[7] C. Fiori, K. Ahn and H. A. Rakha, "Power-based electric vehicle energy consumption model: Model development and validation," in *Applied Energy*, vol. 168, pp. 257-268, 2016, doi: 10.1016/j.apenergy.2016.01.097.

[8] M. Ehsani, Y. Gao, S. E. Gay and A. Emadi, *Modern Electric, Hybrid Electric, and Fuel Cell Vehicles*. Boca Raton, FL: CRC Press, 2005.

[9] T. A. Burress et al., "Evaluation of the 2010 toyota prius hybrid synergy drive system," Oak Ridge Nat. Lab., Oak Ridge, TN, USA, Rep. ORNL/TM-2010/253, 2011.